Rapport de stage
Master 2eme année physique fondamentale

Optical Follower Servo design for the calibration of a gravitational wave detector

Laetitia CANETE

Responsable de stage : Richard Savage

Table of contents

Introduction

Calibration is a crucial and complicated task for large-scale gravitational waves detectors. In the United States, the two LIGO gravitational wave observatories in Louisiana and in Washington State were built to detect perturbations as small as 10^{-18}m over distances of several kilometers. Both observatories are proceeding with equipment updates to be ready for the next generation of operating detectors, the Advanced LIGO (aLIGO), with better performance and sensitivity than the previous versions. With the goal of obtaining the most accurate measurements, the interferometer needs to be accurately calibrated when it is enhanced and running. A dedicated hardware system called the Photon Calibrator subsystem or Pcal was developed for aLIGO and this hardware has an important role to play in the future success of the LIGO project. With 4-km-long optical cavities, many perturbations can affect the interferometer beside gravitational waves and the principal difficulty is to be sure that what we detect is what we want to see – extra-terrestrial gravitational waves.

The entire calibration device is itself subject to noise. It uses a 2-watt laser whose beam needs to be precisely controlled if we wish to erase or at least diminish calibration errors. For this purpose, we have to implement an active controller called the Optical Follower Servo (OFS) that will control and correct the noise affecting the Pcal laser beam, and reduce harmonics induced during generation of the required sinusoidal output power modulations.

In this report, we will detail the requirements of such servo. To motivate our discussion, we will begin with a discussion of gravitational waves and why their detection would have a considerable impact in physics. The calibration subject will bring us then to the experimental issue. The servo, with the aim of reducing the unwanted noise the power of the laser beam has to be simulated to assist in the electronics design before being set up in the Pcal. Its principle of operation, negative feedback control, will be described. Based on the simulation results, a prototype of an OFS was built and the last part of this report will consist of characterization of the OFS and a discussion of its potential for improving the calibration of gravitational wave detectors.

Part I: Gravitational waves and their detection

I.1. A theory of space-time ripples

I.1.1. Einstein's presumptions

The beginning of the twentieth century saw the emergence of a revolutionary theory that deeply changed our understanding of the laws of physics. The framework in which they were built, the space time dimensions, was no longer a fixed grid.

Einstein's general relativity theory (1907-1915) stipulates that space-time was not flat but curved, deformed by mass in such way that we can no longer use Euclidean geometry when we consider large masses over long distances. According to this theory, the gravitational waves would be a manifestation of the space-time deformations in the same way that electromagnetic radiation is a manifestation of moving charges. But whereas electromagnetic radiation can be easily detected due to their interaction with matter, the gravitational waves are almost "invisible." They cross us almost without changing microscopic or even macroscopic properties of matter.

Nevertheless, general relativity theory predicts some characteristic of these gravitational waves. We know for example that they propagate at the speed of light and they are transverse and traceless [1]. As any waves, they propagate with a certain frequency and amplitude, both of which depend on the emitting source.

I.1.2. Sources of gravitational waves

To obtain ripples of space-times, we need asymmetric, accelerating mass distributions. These conditions are easy to fulfill if we do not allow approximations such as saying a planet has a spherical orbit around its star and thus forget about the influence of the planet's mass on the orbit. However, in practice we will consider only significant sources of gravitational waves because the radiation due to systems such as a planet orbiting a star are virtually negligible and undetectable.

If we look farther out into the Universe we can find objects or time-limited phenomena that provide most of the gravitational wave that we wish to intercept.

I.1.2.1. Supernovae

A supernova is the ultimate step in the life of a star with a mass greater than or equal to twelve solar masses. This phenomenon happen when the equilibrium between gravitational force and radiation pressure is broken and the star collapses in a very short time compared to its lifetime, becoming a neutron star or a black hole. This burst will create gravitational waves if the collapse is not spherical and the strength of the radiation will depend mainly on the degree of asymmetry of the supernovae.

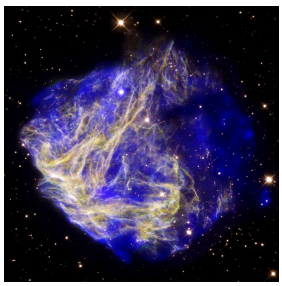

Figure 1: N49 (credit: NASA/STScI/UIUC/Y.H.Chu & R.Williams et al)

I.1.2.2. Coalescence

The orbit of a binary system can decrease into coalescence by radiating gravitational waves. This primarily concerns binary neutron stars and black holes. The radiation we are expecting should have a frequency that increases with the decrease of the distance separating the two objects. Typically the maximum frequency reached by gravitational waves from coalescing binary neutron stars would be 1 kHz and 10kHz/(M*/Msun) for black holes with M* the mass of the heavier of the two objects[1].

I.1.2.3. Pulsars

A pulsar is a young neutron star that has a periodic rotation. If its rotation axis deviates, the pulsar will has a degree of asymmetry and the strength of the gravitational waves emitted will depend of this deviation and of the velocity of the rotation. Unlike the two previous sources considered, pulsars are defined as periodic source because they emit gravitational waves continuously, at almost the same frequency for a long time. The frequency will be directly linked with the rotation's frequency of the star.

I.1.2.4. Stochastic sources

If we sum all sources that we cannot identify and the gravitational waves coming from the Big Bang and the early life of the universe, we obtain a background of radiation that we name the Stochastic Background [2]. Some theories predict that cosmic strings and cosmic super-strings should be at the origin of gravitational waves too. Gravitational radiation from stochastic sources can be considered as a noise if they prevent us from isolating gravitational waves from a particular source.

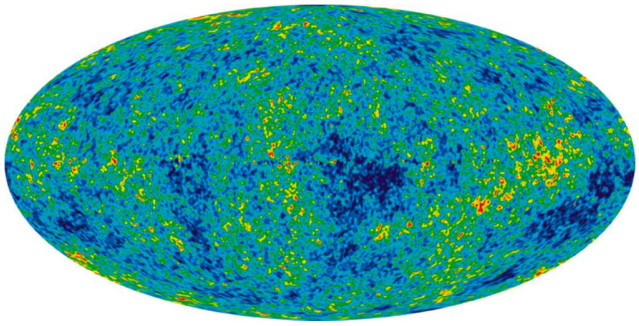

Figure 2: Cosmic background radiation (NASA / WMAP)

I.2. Methods of detection

As we have seen, the existence of gravitational waves is at for this moment mainly theoretical. Mainly, because although we didn't detect a gravitational wave yet by direct measurement of space-time distortion, we already saw proof of their existence. The study of binary pulsar B1913+16 [3] showed that their orbit changed exactly like the model from general relativity of decreasing orbit due to gravitational wave emission had predicted. Thus, we are looking for gravitational radiation in an actual detector to know more about their characteristics. Also, in the same way that the study of radio or microwaves gave us a lot of information about their sources that was 'hidden' in visible light studies, we hope that the analysis of gravitational waves will bring us answers about the composition and evolution of emitting sources. For this purpose different types of detectors were and will be built with different sensitivities depending of the gravitational wave frequency we hope to intercept.

Before entering into the detections field, we have to understand the effect of a gravitational wave crossing matter. For this purpose, we can consider two free masses and look at the relative distance separating the two. If a linearly polarized gravitational wave goes through the plane of the two masses, the proper distance separating the two points will vary. They will not move from their initial place but the space-time where they are defined will be

dilated and contracted. If we consider now a gravitational wave passing through a group of particles in free fall disposed in a circle perpendicular to its direction of propagation, the circle will contract and dilate [4]. The gravitational waves have two polarizations, called + and x, and their effects magnified are show in Figure 3.

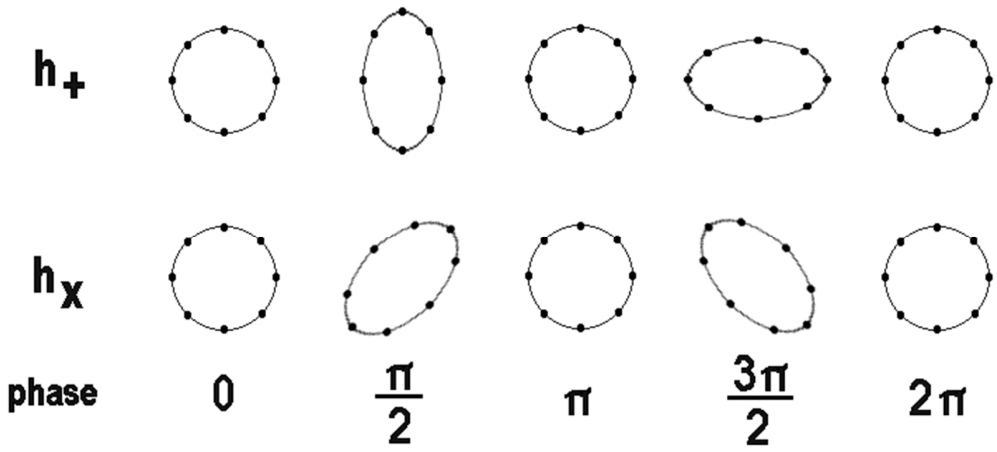

Figure 3: Transit of a gravitational wave over a group of particles (http://www.lmpt.univ-tours.fr/~loic/PDF/encas-gw.pdf)

Hence the aim of the detection field will be to detect this tiny variation of length. Several methods were developed without success so far.

I.2.1. Weber resonant bar

Figure 4: Weber bar at the entrance of the LIGO Hanford Observatory

The first instrument built for the detection of gravitational waves was composed of a large aluminum cylinder weighing approximately 1.5 tons suspended by a steel wire and surrounded by piezoelectric detectors (fig.4). Joseph Weber from the University of Maryland was the inventor of this detector and he endeavored to catch oscillations of the bar caused by distortion of space-time. By the late 60s, he published results and claimed strong evidence of the first detection of gravitational waves. But if we consider the gravitational waves of about 1 kHz from the burst that he wanted to measure with the bar, the variations of the length should have been about 10^{-16} m, barely isolated from noise. Weber's results were invalidated a few years later, but despite this new resonant bars were built around the world, some with exotic materials, often with system for cooling them to cryogenic temperatures. The smallness of the frequency bandwidth that the bar would be able to detect and the absence of results encouraged scientists to look toward a new type of detector, even if some bar detector are still used.

I.2.2. Large terrestrial interferometers

The detection of gravitational waves by interferometers is the method that concentrates the most energy and hope nowadays. They are actually four detectors working, the smallest one is in Hannover (Germany), GEO600, the interferometer VIRGO is at Casina (Italy) and two in the United States that are part of the Laser Interferometer Gravitational Wave Observatory project or LIGO - one in Louisiana and one in Washington State. These detectors have different sensitivities but they all use the same operating principle consisting of analyzing laser interference in Fabry-Perot cavities.

I.2.2.1. Michelson type interferometer

Using a laser rather than a solid material has non-negligible advantages in term of noise. The idea to build such a detector came in the same period of time as the resonant bar studies. However it was not before the early 1990s that full-scale detectors were built. The gravitational waves that these interferometers hope to detect should have a frequency below 10 kHz where the detectors' sensitivities are greatest. They correspond to wavelengths of several dozen kilometers.

A schematic representation of a Michelson interferometer with Fabry-Perot arm cavities is represented in Figure 3. The light of a laser is sent to a beam splitter and is divided into two perpendicular beams. The two enter in cavities through the back surface of a partially transmitting mirror, the corners mass, and go to a reflecting mirror, the end mass, before coming back to the beam splitter. They are recombined and a part will be sent to a photo-detector that will analyze the laser by converting the light into and electric signal and the other part will be sent again to the cavities via a power recycling mirror (not shown). The number of round trips that the light will make will increase the total distance traveled and thus increase the sensitivity.

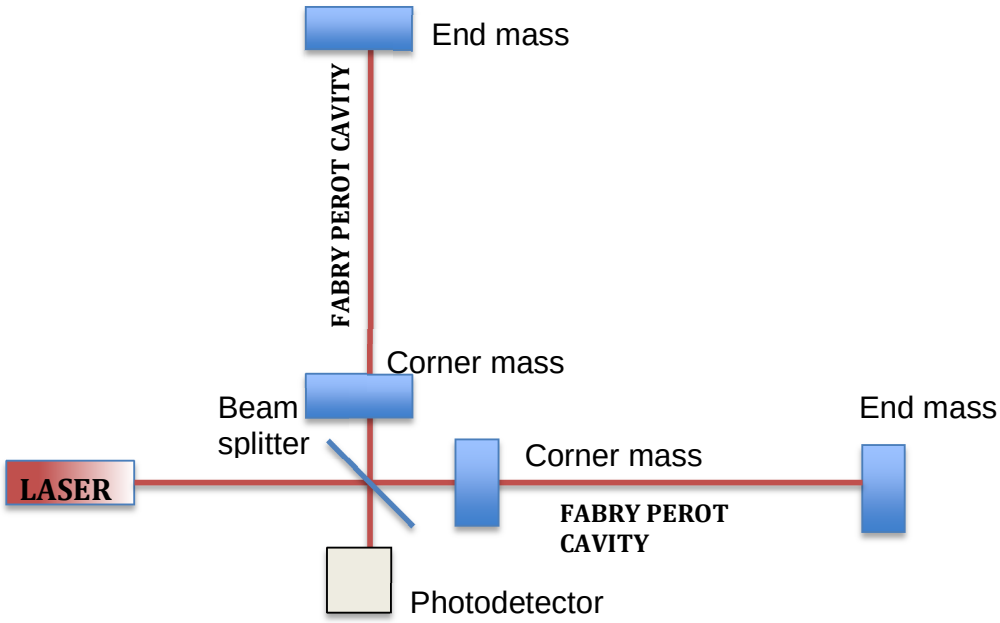

Figure 5: Interferometer with Fabry-Perot cavities

Each arm length is tuned to be as close as possible to a half-integer multiple of the wavelength of the laser used, in sort that the light will be in resonant in the arm cavities. If the length of the arms changes, for example as we expect by the passage of a gravitational waves, the beam will not be in resonance anymore and this phase shift will cause a change in the interference of the light which will be detected by the photodetector [5]

This description is very simplified. Entire books are written on this subject but we can wonder about the interest in building an interferometer like LIGO with long arms of 4 km length. Why can't we settle for a smaller detector where we will just let the beam achieve more round trips in the cavities? In fact one of the biggest problems as we have seen for the resonant bar is to isolate a possible gravitational wave from the noise. They are many causes of noises, they are coming for example from the impossibility to achieve a perfect device, the thermal noise of the mirrors and the wires they are suspended on, or perturbations from outside like seismic noise. Some of the noise sources that affect the gravitational wave amplitude sensitivity scale as about the inverse of the arm's length [1] . Therefore, larger arms will improve the signal to noise ratio of the interferometer.

I.2.2. Space detector

A project from the European Space Agency hopes to launch in the future a detector of gravitational waves called 'NGO' (New Gravitational wave Observer). Composed of three satellites distant by 5 million kilometers from each other, it hopes to be operational for

frequencies from 0.03 mHz to 0.1Hz allowing us to detect waves from various sources like massive black holes binaries, compact object spiraling around black hole, compact binaries and perhaps gravitational waves from the cosmological background.

I.3. Photon calibrators

I.3.1. Aim of calibration

We saw that when we try to detect gravitational waves, we have to deal with noise and find a way for this noise not hide possible gravitational radiation. It is basically the same track as for detection of electromagnetic waves. For example in a radar, the original signal is found by the receiver from a chirp by filtering and demodulation. The chirp condenses the information emitted and always contains noise from electric devices or external interference for example, which need to be separated from the signal. The waveform will be reconstructed and by comparison to the signal emitted, it will be possible to localize the target.

For an interferometer, we have to ensure that the length of the laser is constant around an error margin that is as low as possible. For this purpose, we will first calibrate the detector when is offline to determine the transfer function that converts the variation of length of the laser into an electrical signal [6]. Also when the detector will be online, we want to check continuously that the interferometer is still calibrated. In practice, a Photon calibrator subsystem ('Pcal') will be installed at the end of each arm of the two LIGO interferometers in Hanford and in Livingston. Two generations of detector were already implemented, the Initial LIGO (iLIGO) and the Enhanced LIGO (eLIGO), each with different Pcal installations. The photon calibrators for the Advanced LIGO (aLIGO) era bring the hope of achieving better performance. They will be operational in the near future.

I.3.2. Procedures

The Pcal transmitter module will be placed about 5.7 meters before the end test mass (ETM) of the 4km arms. Two laser beams will be emitted, each with sinusoidal power modulations with controlled frequencies and amplitudes, propagating through window inside the vacuum tube of the arms and reaching the suspended ETM. They will be reflected and collected by a photodetector placed outside the vacuum tube. A schematic of the installation is show in Figure 6:

.

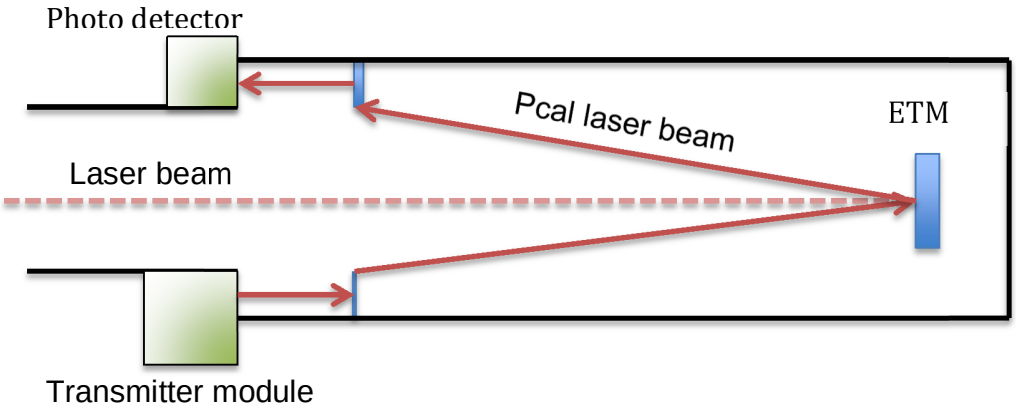

Figure 6: Photon calibrator installation

The transmitter module is composed of a 2W Nd:YLF laser with a wavelength of 1047 nm with an acousto-optic modulator (AOM) driven by an Optical Follower Servo (OFS) to induce sinusoidal power modulation at specified frequencies.
In the vacuum tube, after passing through a system of relay mirrors called the periscope, the laser beam will reach the ETM and induce an oscillation of the mirror position due to the radiation pressure of the photons. Indeed, the beam will transfer momentum from its photons to the mirror. The suspended ETMs have a pendulum resonance of about 0.75 Hz [7] and if the frequency of the laser beam is far above this value, the ETM motion will be approximated by that of a free mass moving in the horizontal plane. From second of Newton's laws $\frac{dp}{dt} = \sum F$, we obtain the amplitude of the induced periodic displacement:

$$x_0 = -\frac{2p_0}{c}\frac{1}{M\omega^2}(cos\theta) \qquad (1)$$

With p_0 the amplitude of the periodic laser power modulation, M the mass of the ETM, c the velocity of light in vacuum, ω the angular frequency of the power modulation and θ the angle of incidence of the laser beam on the mirror. For the purpose of the calibration, this displacement needs to be achieved with a precision of better than 5% [8].

If we refer to this equation, we need a modulation of the laser power that is high enough to induce the required displacement of the ETM. But if the amplitude of the modulation is high, the amplitude of the noise will increase proportionally and might be above the allowed levels. The OFS is intended to be able to diminish the amplitude of this noise.

To obtain a modulation of the signal, we use an acousto-optic modulator (AOM). It is composed of a piezoelectric transducer (PZT) bonded to a transparent crystal that will stretch or contract when it is driven by an electric signal. If the signal is for example sinusoidal, the transducer will stretch and contract and the oscillation of its length will create an acoustic wave that induces an index of refraction grating inside the AOM crystal. If a laser beam is sent through the AOM, it will be diffracted by the acoustic wave-induced index grating. If the amplitude of the sinusoidal drive to the PZT is sinusoidally modulated in amplitude, the signal

received by a photo-detector placed in either the diffracted or non-diffracted beam output will be sinusoidally modulated.

1.3.3. Noise requirement

If the power modulation of the Pcal laser is not perfectly sinusoidal, the induced movement of the ETM due to the Pcal will not be perfectly sinusoidal and it will thereby induce unwanted displacement noise to the ETM. This noise is coming from relative power noise of the laser called RPN and from harmonics created when we modulate the power of the laser with the AOM.

1.3.3.1. The Relative Power Noise

The RPN is inherent to the laser and must not be above a certain limit depending of the frequency. The requirement stipulates that this noise should not induce test mass displacements in excess of 10% of the design sensitivity. The displacement of the ETM caused by power noise is given by [8]:

$$\Delta x = \frac{2\Delta P_{max} cos(\theta)}{Mc\omega^2} \qquad (2)$$

Where $\Delta P_{max} = P_t * RPN$, with P_t the total power incident of the laser beam on the ETM. Following the requirements:

$$\Delta x \leq Lh(f)/10$$

With h(f) the design strain sensitivity and L the length of the arm. Therefore the maximum value of the RPN will be:

$$RPN_{max} = \frac{Mc\omega^2 Lh(f)}{20 P_t \cos(\theta)} \qquad (3)$$

The free-running RPN measured without the OFS is show in Figure 7. In this diagram, the requirement is named 'Zero-DetHighP' and we see that it is exceeded by the laser beam at frequencies below 70 Hz. The OFS would have to reduce the RPN by about 15-20 dB up to this frequency.

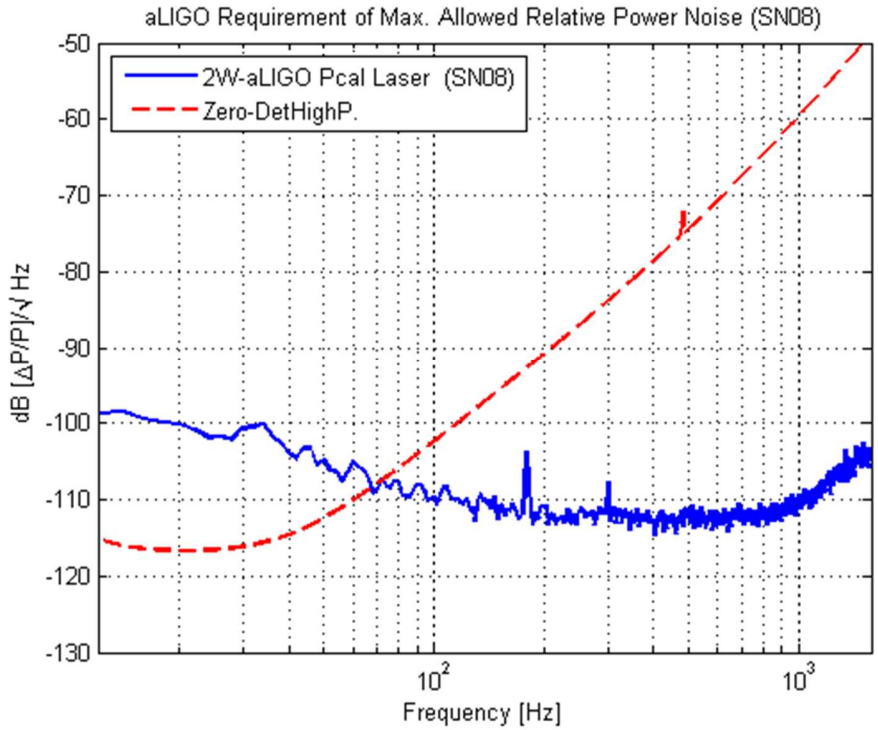

Figure 7: RPN of the laser beam compared to the requirement

1.3.3.2. Harmonics noise

The harmonics noise is due to the non-linearity of the modulation process. It induces a displacement of the ETM that has to be less than 1/10 of the design sensitivity. The amplitude of this displacement depend of the order n of the harmonics considered. It will decrease by a factor n^2.

In the same time, we want the carriers induce a displacement of about 20 time the design sensitivity. So the harmonics amplitudes in respect to the carrier amplitude would be about:

$$\frac{\Delta P(2f_0)}{\Delta P(f_0)} < \frac{1}{50} = -34\ dBc \quad \text{for the first harmonic}$$

$$\frac{\Delta P(3f_0)}{\Delta P(f_0)} < \frac{9}{200} = -27\ dBc \quad \text{for the second harmonic}$$

Therefore, for all the harmonics:

$$\frac{\Delta P(nf_0)}{\Delta P(f_0)} < \frac{n^2}{200} \qquad (4)$$

The figure 8 illustrate this requirement. The 'zero detuning high power' plots show the maximal harmonics amplitude we want to achieve.

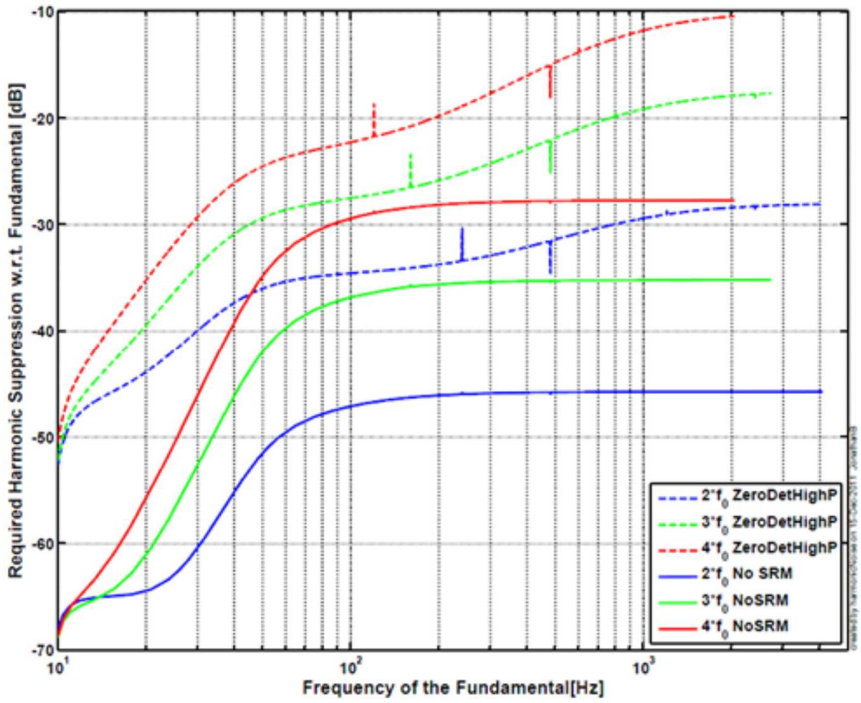

Figure 8: Maximum allowable relative harmonic noise in respect to the fundamental (Jonathan Berliner- https://dcc.ligo.org/DocDB/0032/T1100068/020/PhotonCalibratorFinalDesign.pdf)

We did tests using the laser and an AOM to see how far we are from these requirements. The AOM driver has a video input that controls the amplitude of the 80 MHz sine wave that drives the AOM. The Pcal uses this video input to modulate the power diffracted by the AOM. For this purpose, we first determined the half DC voltage (or offset) by raising the voltage sent through the AOM video input until the diffracted power reached the maximum value (Fig.9).

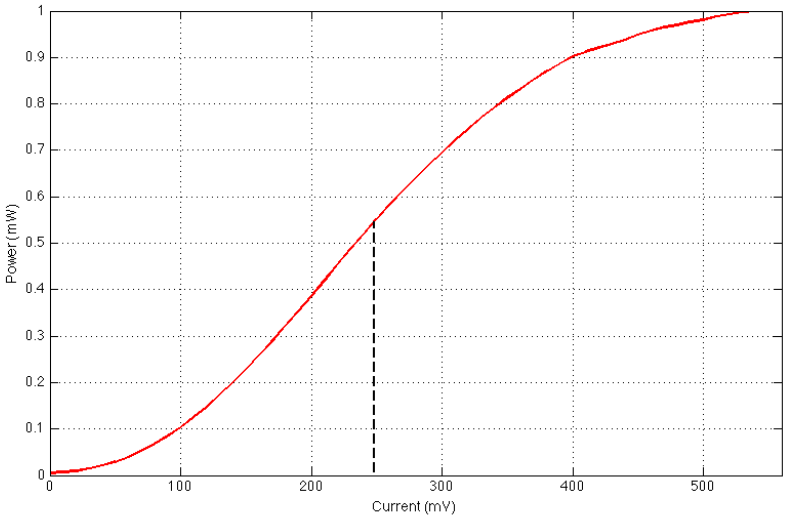

Figure 9: Power in function of the signal current

We keep the offset corresponding to half the value of the maximum power and we obtained approximately 250 mV. Then, we modulated the power of the laser beam diffracted by the AOM by injecting a sinusoidal signal into the video input with amplitude equal to a percentage of the half DC voltage. We choose four different frequencies for this signal, 50 Hz, 400 Hz, 1.1 kHz and 2 kHz that are the nominal 'Calibrations Line' frequencies [8].

To obtain the magnitude of the harmonics as a function of the carrier frequency we used an audio analyzer that made a Fast Fourier Transform (FFT) of the signal studied. Some plots of the data are included in Appendix II. If we compare these results with the requirements, we see that only for small modulation the requirements are fulfilled (Fig.10).

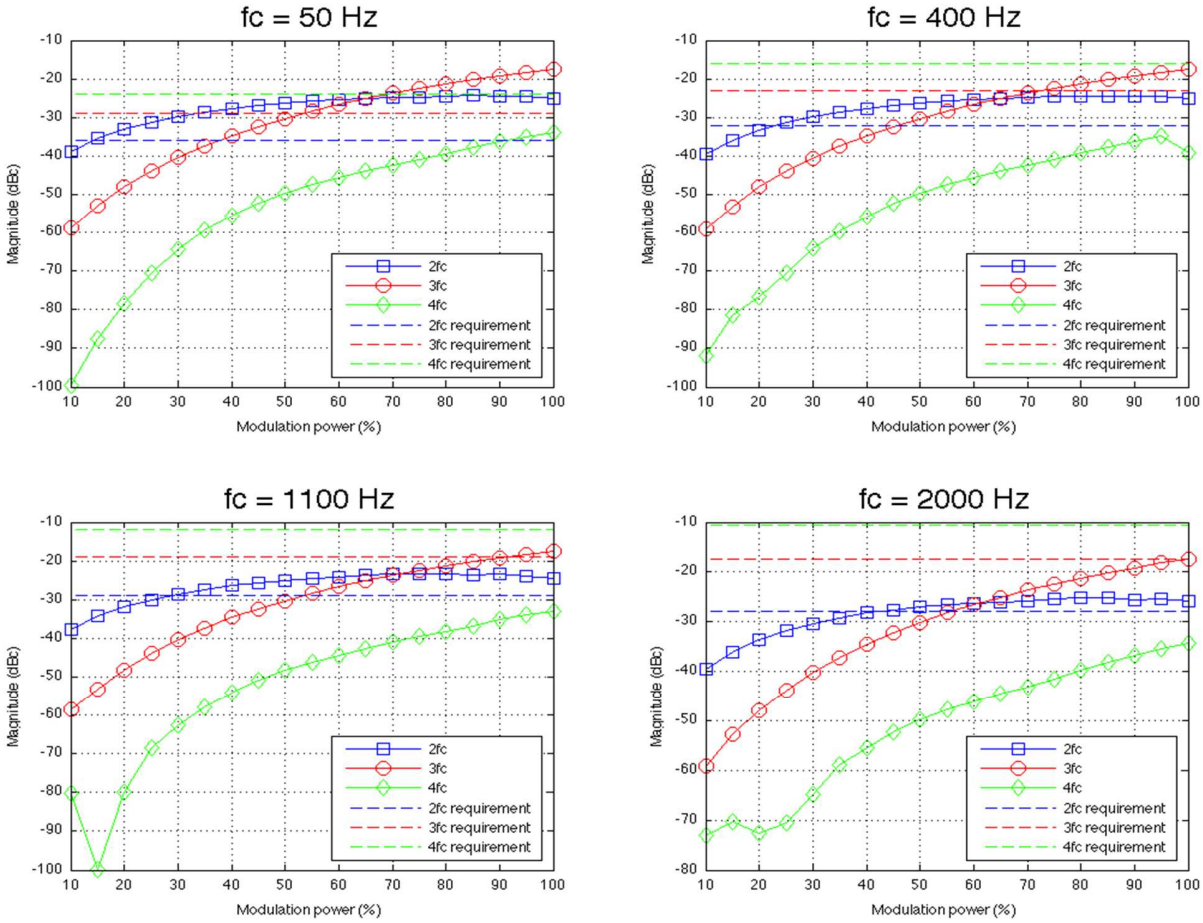

Figure 10: Relative amplitude of the harmonics for different modulations

We observe that the amplitude of 3fc is higher than the amplitudes of 2fc and 4fc for high modulation. In fact, the harder we modulate the laser power the closer the shape of the power modulation approximates a square wave. A simple Fourier analysis shows that a square wave is composed only of odd harmonics from a sinusoid[1]. In the Pcal, the OFS will reduce the magnitude of the harmonics for high modulation.

[1] See Appendix III

Part II: Optical Follower Servo implementation

II.1. Feedback control

II.1.1 Feedback system

An Optical Follower Servo is a dynamic electric device that has the particularity to control a signal using a feedback system. The idea of feedback is to link several systems together in such a way that they are coupled to each other. In this manner, we can compare and bring a signal close to a reference. This is the basic operating principle of a thermostat. A thermometer measures a temperature and compare it to a reference, the temperature we want. If it's under this value, the heat is turned on and when the temperature of the room reaches the reference, the heat is turned off.

To illustrate a feedback system, we generally use a block diagram that assign to each component of the system a block that we connect in open or closed loop configuration depending of which output we want to obtain (Fig.10).

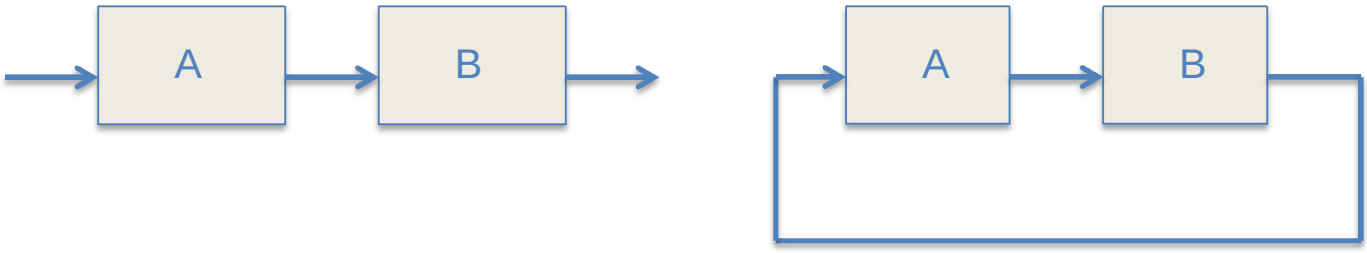

(a) (b)

Figure 11: Block diagrams: (a) Open loop and (b) closed loop. The arrows go from output to input of the systems.

We observe that in the closed loop, the output of block B is bound to the input of block A. In this configuration we have feedback control. This feedback can be positive or negative. If we take

again our example, in the closed loop we can add or substrate the signal from output B with another signal:

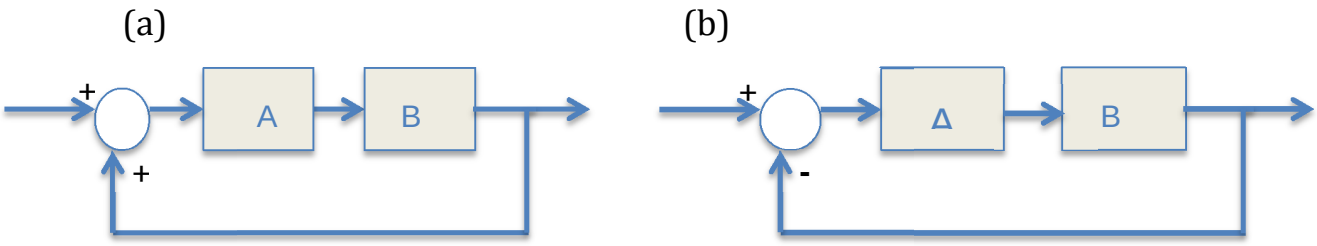

Figure 12: (a) Positive feedback. (b) Negative feedback

By changing one sign, we obtain two opposite effects. In a positive feedback system, a signal that increase will increase further, up to saturation [10]. It is not used very often, although it is present in biological systems. In negative feedback, the increase or decrease of a signal will be controlled and/or diminished by the loop.

II.1.2. Transfer function and Bode diagrams

II.1.2.1. Relation between Block diagram and transfer function

The equation that links the output and the input of a linear system is called the transfer function. Knowing the input signal of a system and its transfer function, we can determine- depending of what we are looking for- the amplitude or the frequency of the signal at the output of the system.

From a block diagram, it's easy to define the transfer function of a system by simplifying the diagram if necessary. For example, Figure 11 a) can be transformed in such way the final diagram will contain only one block. For this system the transfer function will be given by:

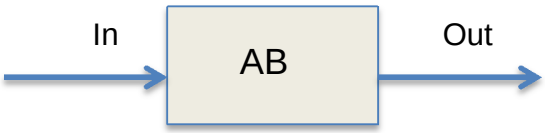

$$\frac{Out}{In} = AB$$

Another very common case will be to have two or more blocks in parallel. The transfer function of such a closed loop is:

$$\frac{Out}{In} = \frac{A}{AB \mp 1}$$

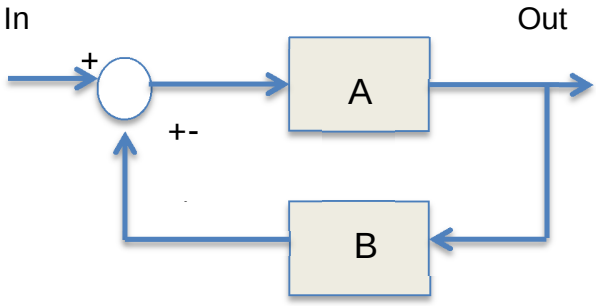

Here the choice of sign depends on whether we have a positive or negative feedback as we have seen above. The minus sign will be for a negative feedback and the plus for a positive feedback.

II.1.2.2. The frequency domain

When we look to the evolution of a system, we can basically use the time as a variable reference. But in signal processing and study of feedback systems, we need often to refer to the frequency domain for example to check the periodicity of a signal or to measure its harmonics. One technique used to convert a time-dependent function into the frequency domain is the Laplace transform. If f(t) is a function of time and t>0, the Laplace transform can be defined as:

$$\mathcal{L}[f(t)] \equiv \int_{0+}^{\infty} f(t)e^{-st}dt \qquad (5)$$

With s a variable that contain a real and a complex part: s=Re(s)+iIm(s) or s=iω in the case of physical frequencies. Thus, f is now a function of s and we will call it F[s]. To evaluate physical frequencies, we set Im(s)=ω where ω is the angular frequency that is defined by: ω=2πf. In Appendix IV, we give results of Laplace transforms for some typical functions encountered.

The transfer function of a system is usually given in the frequency domain and it is in the form [11]:

$$T(s) = \frac{a_m s^m + a_{m-1}s^{m-1} + \cdots a_0}{s^n + b_{n-1}s^{n-1} + \cdots b_0} \qquad (6)$$

or,

$$T(s) = a_m \frac{\prod_{k=1}^{m}(s - Z_k)}{\prod_{l=1}^{n}(s - P_l)} \qquad (7)$$

where 0<=m<=n are integer numbers, a_0...a_m and b_0...b_m are real numbers and by definition Z_1...Z_m are the zeros, and P_1....P_m the poles of the transfer function. These numbers play a very important rule when we try to characterize the behavior of a system, as we shall see by looking at the magnitude and phase of the transfer function in a Bode diagram.

II.1.2.3. Bode analysis

a. A simple example: a low pass filter

To illustrate our discussion in this chapter, we will consider first a widely used device that is present in the Optical Follower Servo, a low pass filter. It can be one block of Figure 12 for example. Basically, its operating principle is to reduce the amplitude of a signal as the signal frequency increases. The transfer function of a first-order low pass filter is:

$$T_1(s) = \frac{a_0}{s - P_1} \qquad (8)$$

With a_0 the gain and P_1 the pole of the function. For a second order low pass filter, we have two poles:

$$T_2(s) = \frac{a_0}{(s - P_1)(s - P_2)} \qquad (9)$$

We can increase the order by incrementing n in the equation (6). In practice by raising the order in a low pass filter, the amplitude of the higher frequencies will decrease faster.

In order to study the stability of a system we can, from the transfer functions, compute the magnitude and the phase. Indeed T(s) is a complex number and by definition:

$$Magnitude = \sqrt{|T(s)T(s)^*|}$$

$$Phase = \arctan\left(\frac{Im\big(T(s)\big)}{Re\big(T(s)\big)}\right)$$

If we plot the magnitude and the phase versus the angular frequency, we obtain a Bode diagram. The magnitude will usually be expressed in dB, and voltages are converted to these units by: $[dB]=20\log([V_{out}/V_{\_in}])$.

Let's see what we obtain with a low pass filter generated using Matlab and Simulink:

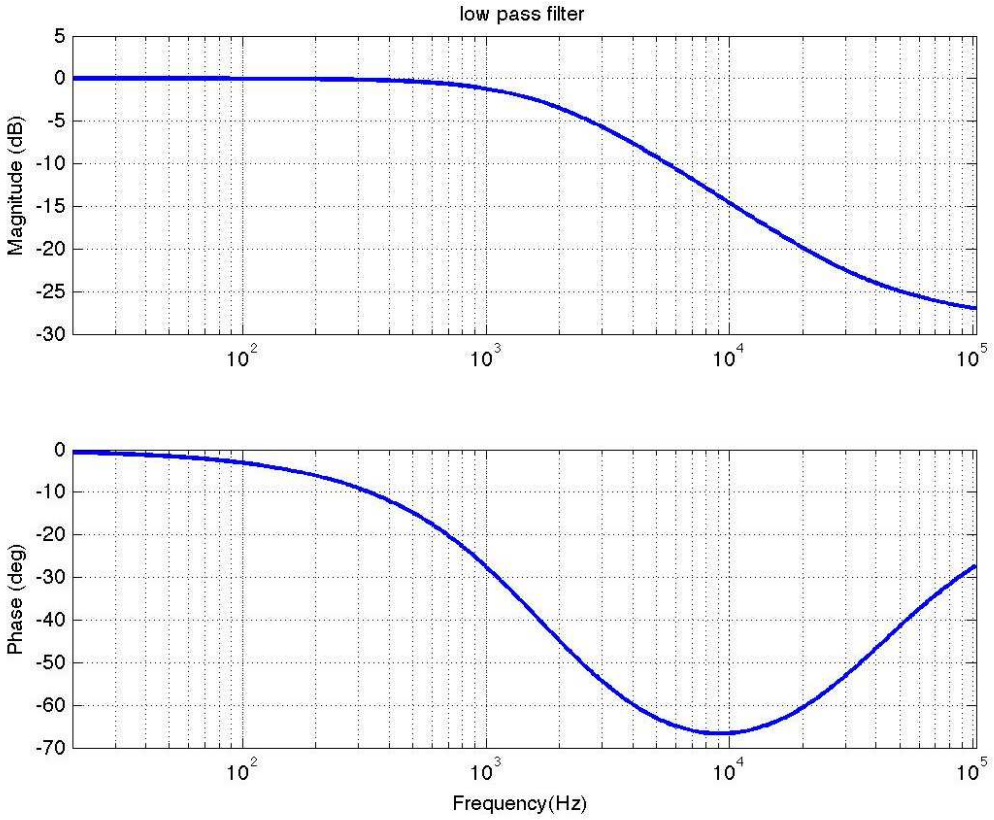

Figure 13: Bode diagram of a low pass filter

We injected a sinusoidal signal with a frequency varying from 20 Hz to 102 kHz through the low pass filter. We see as we expected that the magnitude of the signal decreases for high frequencies. In practice, the bandwidth will depend to the value of the components we choose to build the low pass filter. An electronics schematic of the Optical Follower Servo is included in Appendix V.

The pole frequency of the transfer function defined in equation (8) can be easily determined by looking at the plot of the magnitude. It is equal to what we call the corner frequency. It corresponds to the frequency of the point where the magnitude decreases by 3 dB from its maximal value. With the low pass filter used, the corner frequency is approximately 2 kHz and the magnitude after this point decrease by 20 dB per decade. Furthermore, for a stable first order system, the phase must be equal to -45° at the corner frequency. We see that is effectively the case for our filter.

We could see other correspondences between the magnitude and phase diagrams. In fact in some cases, we can predict the behavior of the phase knowing the magnitude and inversely by using the Kramers Kronig relations.

b. The Bode relations

The complex and real part of an analytic function in the upper half plane[2] can be connected using the Kramers Kronig relations. Thus, if we split the transfer function into real and imaginary parts, we obtain:

$$T(\omega) = T'(\omega) + iT''(\omega)$$

If T'(ω) and T''(ω) are real and if T(ω) vanishes faster than $1/|\omega|$ for large ω, we can write:

$$T'(\omega) = \frac{2}{\pi} P \int_0^{\infty} \frac{\omega' T''(\omega')}{\omega'^2 - \omega^2} d\omega' \qquad (10a)$$

$$T''(\omega) = \frac{-2\omega}{\pi} P \int_0^{\infty} \frac{T\prime(\omega')}{(\omega'^2 - \omega^2)} d\omega' \qquad (10b)$$

with P the Cauchy principal value[3]. These two equations are the Kramers Kronig relations. If now we set:

$\ln T(\omega) = \ln|T(\omega)| + i \times \arg(T(\omega))$, we obtain from (10b):

$$\arg\big(T(\omega)\big) = \left(\frac{-2\omega}{\pi}\right) P \int_0^{\infty} \frac{\ln|T(\omega')|}{(\omega'^2 - \omega^2)} d\omega' \qquad (11)$$

After some mathematical developments that we will skip here, we obtain the Bode relation:

$$\arg\big(T(\omega)\big) = \frac{-\pi}{2} \int_{-\infty}^{\infty} f(v) \frac{dln|T(\omega')|}{dv} dv$$

$$\sim \frac{-\pi}{2} \frac{dln|T(\omega)|}{dln(\omega)} \qquad (12)$$

where $f(v) = \frac{2}{\pi^2} \ln \coth\left[\frac{|v|}{2}\right]$ and $v = ln\left(\frac{\omega\prime}{\omega}\right)$. If the slope of the gain curve is constant and equal to n, the phase curve will be:

$$\arg\big(G(\omega)\big) = \frac{n\pi}{2} \qquad (13)$$

[2] If we consider a plane with the real numbers in the abscissa and the complex numbers in the ordinate, the upper half plane will be composed of numbers real and complex positive.

[3] The Cauchy principal value is a number associated to a limit of the integral of a function.

The Bode relations have restrictions coming from the conditions under which we can apply the Kramers Kronig relations. The response function must not possess poles and zeros in the right half plane. Systems that fulfill this requirement are called *minimum-phase* systems [13]. If they possess poles and/or zeros in the right half plane, it means they have a phase lag. This delay cannot be predicted by Bode relations. Response functions that are in this case are called *non-minimum phase*. Such systems are quite common and include for example all systems with a time delay.

II.2. Servo design

II.2.1. General presentation

The Optical Follower Servo closed loop configuration can be represented in the form of a Block diagram (Fig.11):

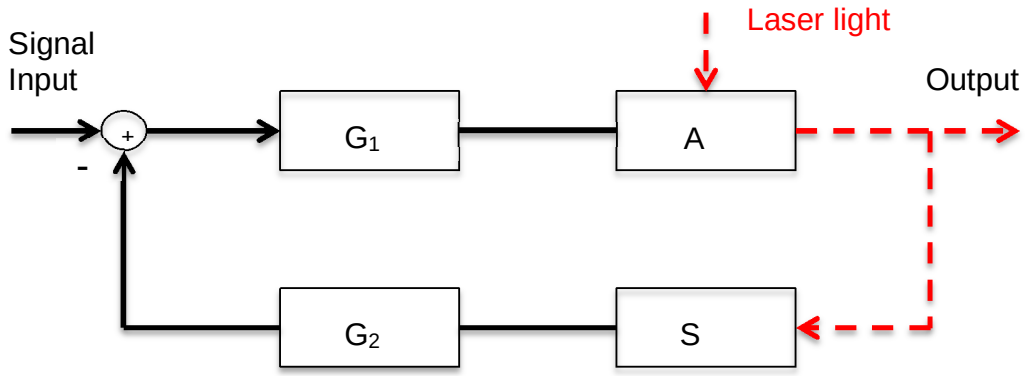

Figure 14: OFS Block diagram representation

Schematically, about one percent of the laser beam enters in the actuator (A), an acousto-optic modulator that will modulate the power of the beam (see 1.3.3.2). The light then will pass through a photodiode (S) that will convert the beam into an electric signal. The amplitude of this signal is increased by a gain (G_2) and then will be subtracted from the input, the reference waveform. The new signal obtained is amplified by a variable gain (G_1) and sent to the AOM. Thus we see that the OFS is a feedback system, and we can set the transfer function of the closed loop of this system as:

$$T = \frac{AG_1}{1+SAG_1G_2} \qquad (14)$$

This transfer function can be reduced by choosing the value of G_2 in such way that we obtain $SG_2 \sim 1$ and so:

$$T = \frac{AG_1}{1+AG_1} \qquad (15)$$

This scheme gives the important components of the Servo. In order to implement the OFS, we have to determine the poles and the zeros of this system by simulation before building a prototype.

II.2.2 Simulation of a model

II.2.2.1. Requirements

By changing the poles and zero of the Servo, we can modify the transfer function. In Figure 7, we saw that to fulfill the requirement we have to reduce the relative power noise of the laser beam by approximately 20 dB up to 100 kHz. Also, because we know we need a finite loop bandwidth, we want that the gain fall to 0 dB at about 100 kHz in the transfer function of the OFS. For good loop performance, the gain should be as high as possible below 5 kHz. This value is chosen considering that the maximum calibration line frequency is about 2 kHz. We take twice this frequency and we keep a value a little above for a safety margin.
The stability of our system can be checked by computing the phase margin of the open loop transfer function [12]. This value is straightforward to find by looking the Bode plot representation of the open loop. We take the phase corresponding to the frequency of the unity gain and we add 180° to this value. To illustrate this concept, a transfer function is plotted on a polar diagram (Fig. 15). For a magnitude equal to 1, the curve follow an unit circle and its angle with respect to the real axis will depend on the definition of the value of the phase.

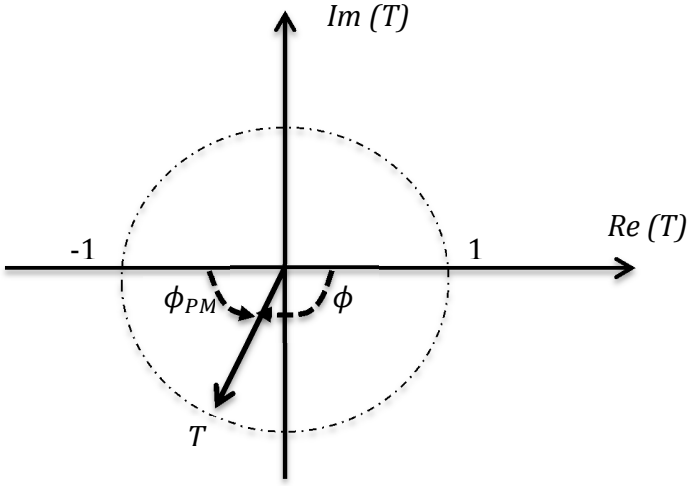

Figure 15: Polar plot of a transfer function at unity gain

The phase margin will be the angle between T and the point (-1,0). To achieve the best relative stability, we want the phase margin to be has high as possible, at least 50 deg.

Considering these requirements, we choose a transfer function with two poles and one zero, thus a second order transfer function. Indeed, by increasing the order, the plot of the magnitude will have a steeper slope and so the curve will reach the unity gain at a smaller frequency. But good stability will be harder to achieve for a high order transfer function, so the second order is a good compromise. If we add more poles, the phase margin will get worse. Therefore, the normalized transfer function will be:

$$T(s) = \frac{(s+\omega_z)\omega_p^2}{(s+\omega_p)^2\omega_z} \qquad (16)$$

with $s = i\omega$

II.2.2.2. Modeling

A simulation of the OFS can be achieved using Matlab and Simulink software. Thereby, we can easily try different poles and zeros, and check how the stability of the OFS is affected by plotting Bode diagrams.

The final configuration obtained is presented in Appendix VI. In this model, the loop can be open or closed using a manual switch. Different outputs are set to test different parts of the feedback system. For example when the loop is open, we check the AC transfer function from the reference signal to the error point, test 1. With the AC coupling, we will remove the DC component from the injected signal. The Bode plot obtained from error test point 1 is shown in Figure 16.

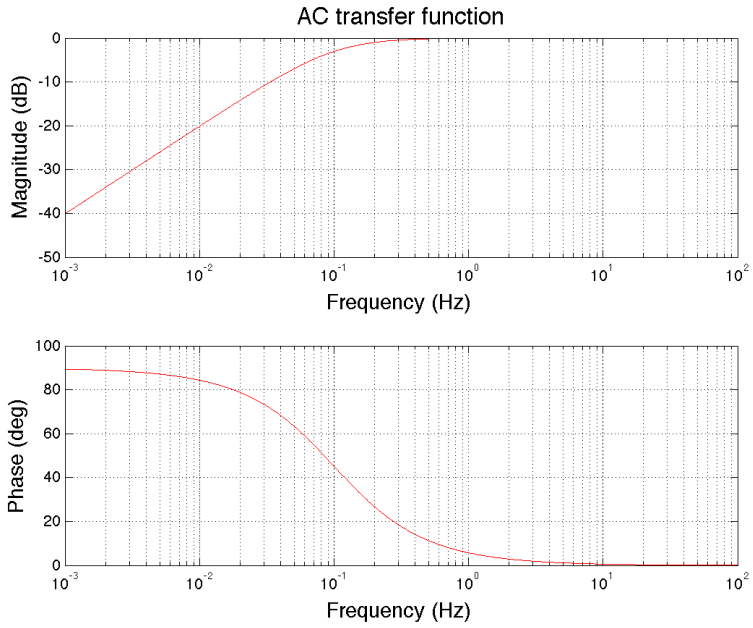

Figure 16: Bode plot of the AC coupling with a zero at DC and a pole at 0.1 Hz

The block named 'Servo electronics' will be used to define the zero and poles of the servo. In practice, it will contain an operational amplifier, resistors and capacitors in a circuit that will act as a second order active filter with a gain (Fig 17).

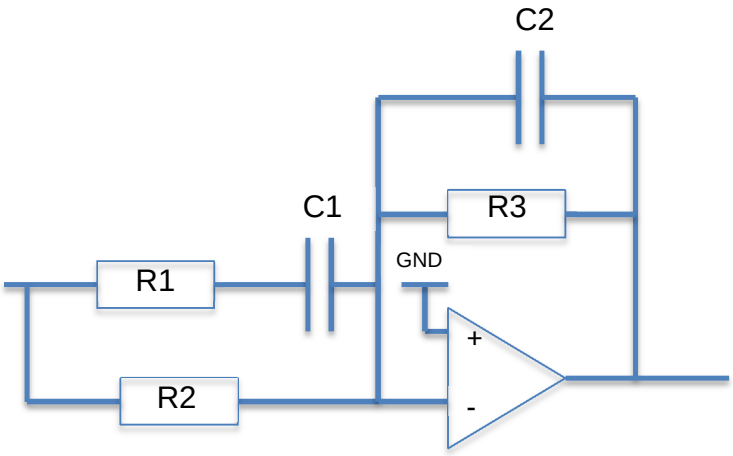

Figure 17: Inside 'Servo electronics' box

When we start the simulation, we don't know the value of the poles and zero of the "Servo electronics." From what we said in the first part of the simulation chapter, we will run the Simulink model for different poles and zeros and see which Bode plots will better fulfill the

requirements. We will look around nominal values of 10 kHz for the poles and 80 kHz for the zero. For the poles, this value was chosen because we don't want the gain to decrease too much before 5 kHz. The choice of the nominal value of the zero was made by testing the loop for different values. By increasing the zero, the unity gain frequency and the phase margin decreases.

With the Matlab code, we plot Bode diagrams for a zero frequency range from 40 kHz to 120 kHz and a unity gain frequency (UGF) at 100 kHz. According to equation (16), each zero frequency corresponds to a pole frequency:

$$\omega_p = \frac{\omega}{\sqrt{100\sqrt{A}-1}} \qquad (17)$$

with $A = \frac{\omega^2+\omega_Z^2}{\omega_Z^2}$ and $\omega = 2\pi UGF$.

The relation that links the pole and the zero frequencies is plotted in Figure. 18.

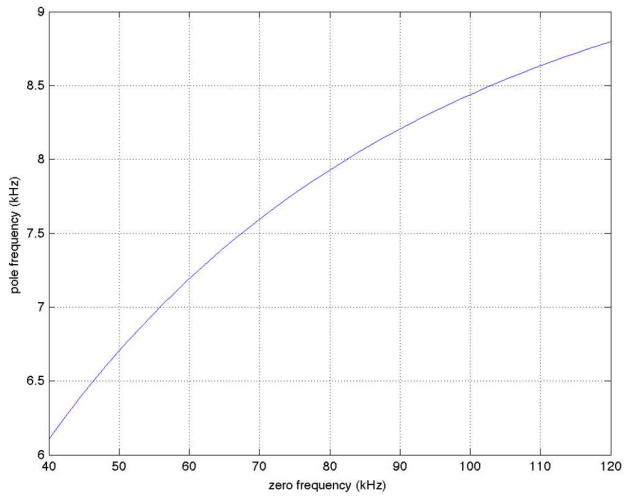

Figure 18: Pole frequencies in function to zero frequencies

II.2.2.3. Results of the simulation

We first plot the Bode diagram of the Servo for 10 zero frequency values[4]:

[4] Plots for 50 different frequency values are included in Appendix VII.

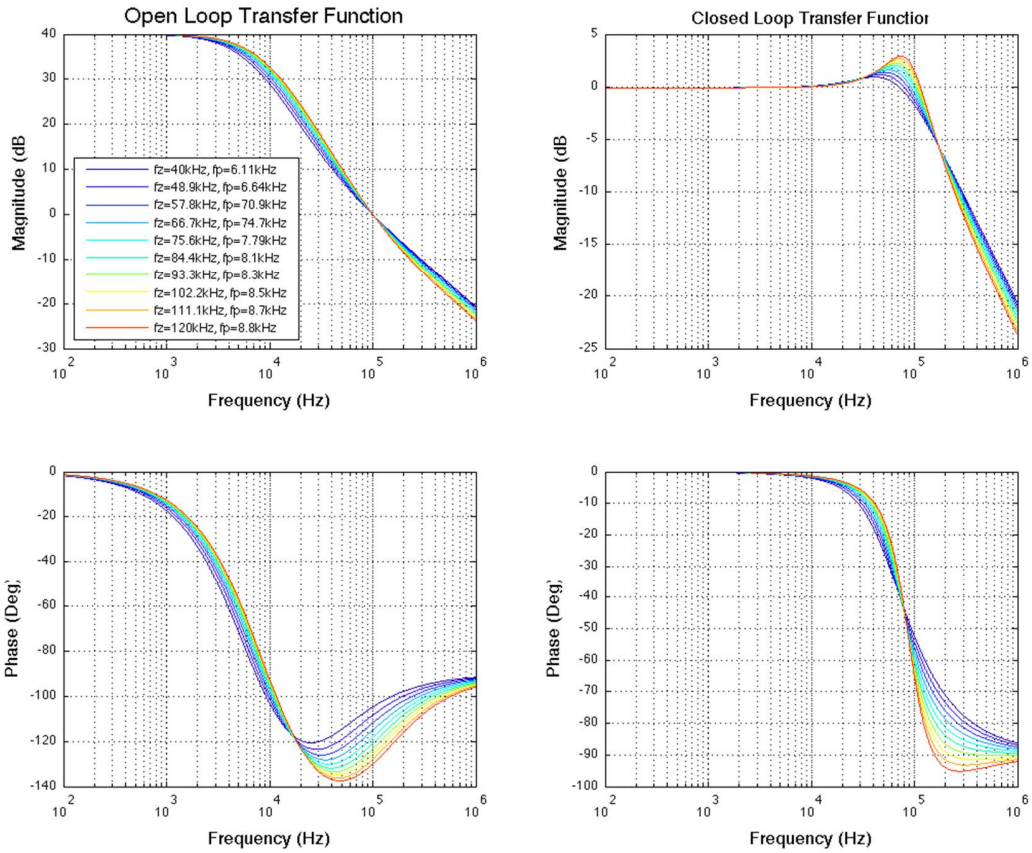

Figure 19: Bode diagrams for 10 zero frequencies

From Figure 20, we can check the phase margin of the open loop transfer function and the flatness of the closed loop transfer function:

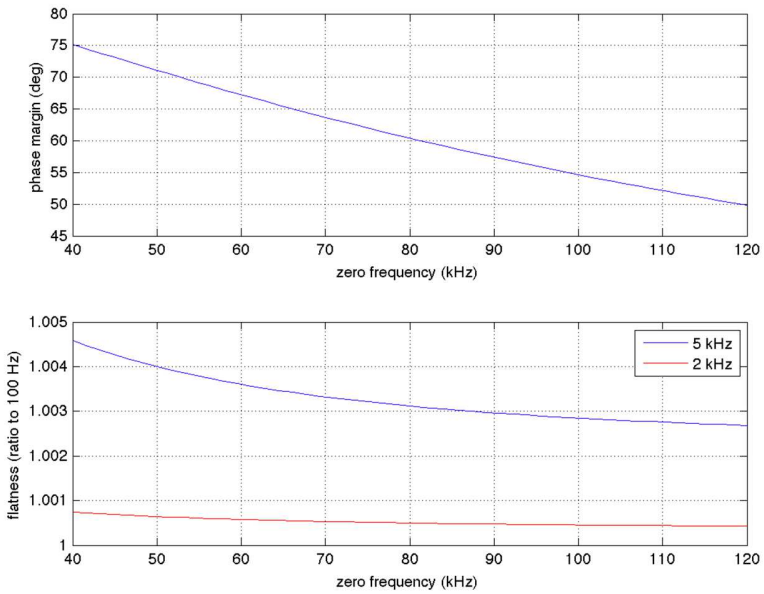

Figure 20: Phase margin and flatness as a function of the zero frequency

We don't want the zero frequency too high because we see that the phase margin gets bad. But if we choose a zero frequency too low, the flatness ratio become high. For stability, a reasonable phase margin is 60 deg. For this value, the zero frequency is 80 kHz and the flatness error for 5 kHz would be around 0.3% so a good compromise is achieved. From Figure 18, we see that this zero corresponds to a pole frequency of approximately 7.9 kHz.
Using these values in the Simulink model of the Servo, we can now check that the Bode plots will fulfill the requirements. The open loop result is given in Appendix VIII. When we close the loop, we obtain the transfer function plotted in Figure 21.

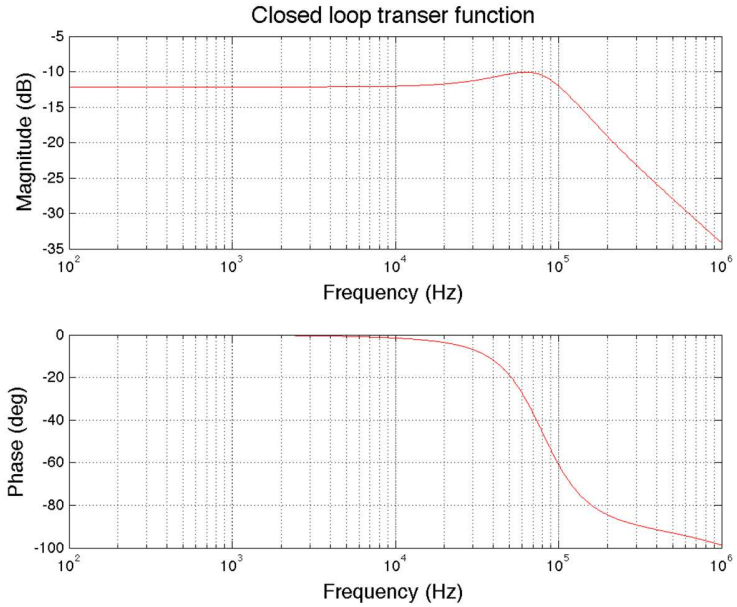

Figure 21: Closed loop transfer function of the OFS model

As we expected, we see that at 5 kHz, the slope is flat and the maximum gain peaking is less than 2dB. The Optical Follower Servo that we will realize for the photon calibrator should have a zero frequency at 80 kHz and pole frequency at 7.9 kHz.

II.3. Test of a OFS prototype

II.3.1. Procedures

Now that we have a precise idea of what the Servo is composed of and of its component parameters, we have to build a real prototype to compare its performance with the results obtained by simulation. A picture of the first-article module is represented in Figure 22.

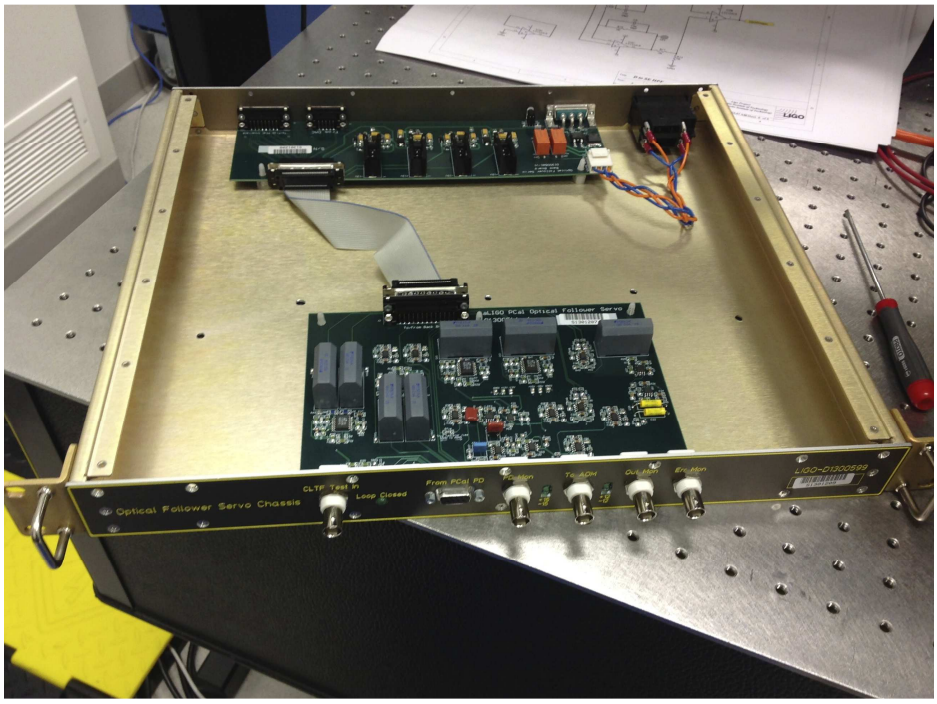

Figure 22: First-article Optical Follower Servo

The first step is to power up the servo and check if it's operating. It is powered by a DC voltage of 18V. The loop can be closed by sending a 15 V signal to a specific pin of a connector on the servo chassis. The photodetector can be connected directly to the servo or go first to an interface box to obtain a DC-coupled monitor of its output. It can be used to analyze the laser beam directly or by using an integrating sphere.

Before connecting the servo output to the AOM driver, we can first look to the signal obtained and compare to a reference. In this manner, we can see if the Servo is locked.

Then, we have to test the transfer function of the Servo electronic. We send a signal through the Servo and we analyze it with an audio analyzer. We can varied the gain from 6 dB to 26 dB with an external source.

When we will be sure that the servo react as we expect, we can test it for RPN and harmonic noise suppression by using the actuator.

II.3.2. Issues encountered

At first, we saw that the signal from the photodetector was added, not substrated from the reference waveform, thus we had a positive feedback rather than a negative feedback servo loop. To resolve this problem, we inversed the polarity of the signal in such way that the signal from the PD is inverted (see Appendix IX)

The Servo electronics transfer function was close to, but not exactly what we expected. It appears that the phase margin is not as much as we expected which means that the system has more gain peaking at the unity gain frequency (Fig.23) and the unity gain frequency is lower

than what we want. Due to the poor phase margin, we were only able to increase the unity gain frequency to approximately 36 kHz. More detailed measurements revealed a time delay in the circuit.

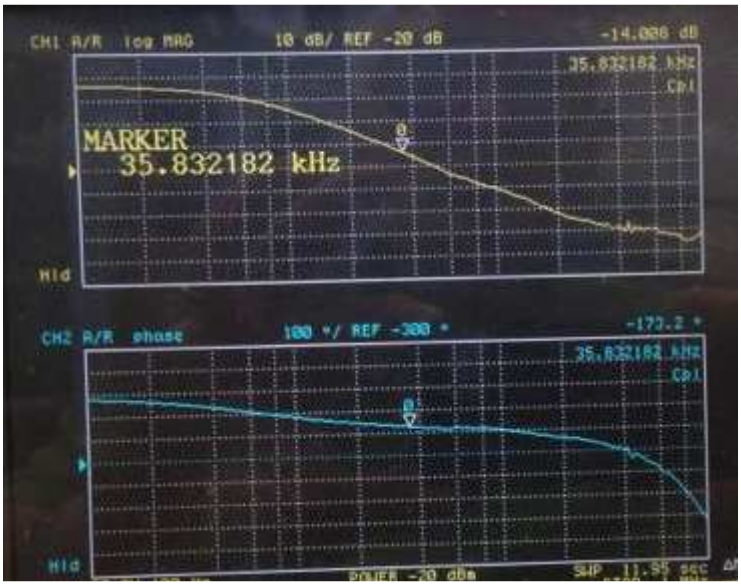

Figure 23: Open loop transfer function of the OFS electronics with a variable gain stage voltage of -0.5 V.

When we try to run the Servo with the actuator (AOM), we found a time delay of about 1 μs. By adjusting the laser beam closer to the AOM transducer, we successfully reduced the delay by about 40%.

II.3.3. Results

After adjusting the beam position in the AOM, we used a dynamic signal analyzer to find the open loop transfer function of the OFS. The unity gain frequency obtained was 75 kHz, the phase margin was 24°, and the gain at low frequency was 40 dB as show on Figure 24:

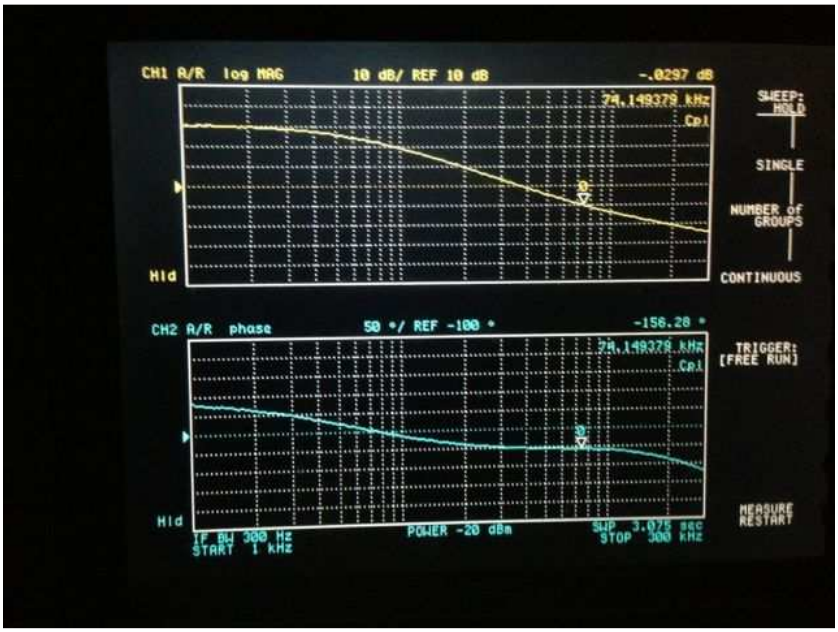

Figure 24: Opel loop transfer function of the OFS after repositioning the beam in the AOM.

The phase margin is still lower than desired, but we decided to try to test the Servo for RPN suppression at low frequency. In Figure 25, we compare the RPN measurements with and without the Servo.

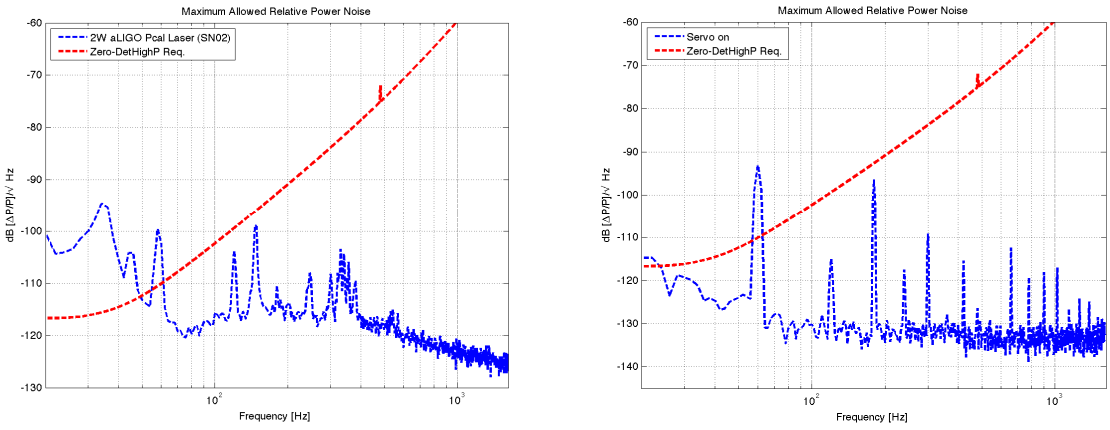

Figure 24: RPN without the servo (on the left) and with the Servo (on the right)

In these plots we see that the RPN is reduced at low frequencies with the Servo on, and the requirement is met at almost all frequencies. We still have to deal with a peak of approximately -94 dB at 60 kHz. This is likely due to grounding issues with our temporary test setup.

Conclusion

Matlab and Simulink simulations gave us a basis on which we were able to design and build an Optical Follower Servo. Like all new devices, the prototype needed to be tested and a several issues addressed before we could compare measurements with the simulation results. We were able to lock the servo (close the loop) and obtain the open- and closed-loop transfer functions. RPN was suppressed below the required level. We have not yet made careful measurement of the harmonic noise suppression, but the first results looks promising. The next step will be to achieve better phase margin, perhaps by further reducing the AOM time delay. The lack in phase margin could come to a defect in the photodetector circuit. We will have to further characterize and eventually implement modifications to the circuit of this device to achieve better phase margin and thus a higher unity gain frequency.

Once this step is done, we can continue to evaluate the ability of the OFS to reduce RPN and harmonics noise. If the prototype meets our requirements, the fabrication of more OFS modules will start in order to equip each transmitter module placed at the end of each of the arms of the three LIGO interferometers.

The LIGO Scientific Collaboration expects to run the advanced version of the interferometers next year and begin efforts to improve the sensitivity to the designed levels to give the best prospects for the first direct detection of gravitational waves. Precise and accurate calibration will be crucial for achieving this goal and it appears that the Optical Follower Servo of the Photon Calibrator will capable of helping to ensure that displacement noise induced by the calibration forces will not compromise this effort.

Acknowledgements

I would particularly thank you my supervisor during this internship, Dr.Richard Savage, for offering me the opportunity to work in the Pcal team and for his valuable help and advices. I was also very kindly welcomed during my stay at Richland by him and his family.

I also thank LIGO Hanford staff for giving me access to the facilities of the site and for their disponibilities.

I would like to thank my coworkers Gregorio Tellez and Pablo Daveloza for their good moods and for sharing their knowledge with me, and Filiberto Clara for his help in electronics lab.

Finally, I placed my gratitude to Dr. Raffaele Flaminio for helping me to find this internship and for putting me in touch with Richard Savage.

Appendicies

I. Transmitter module

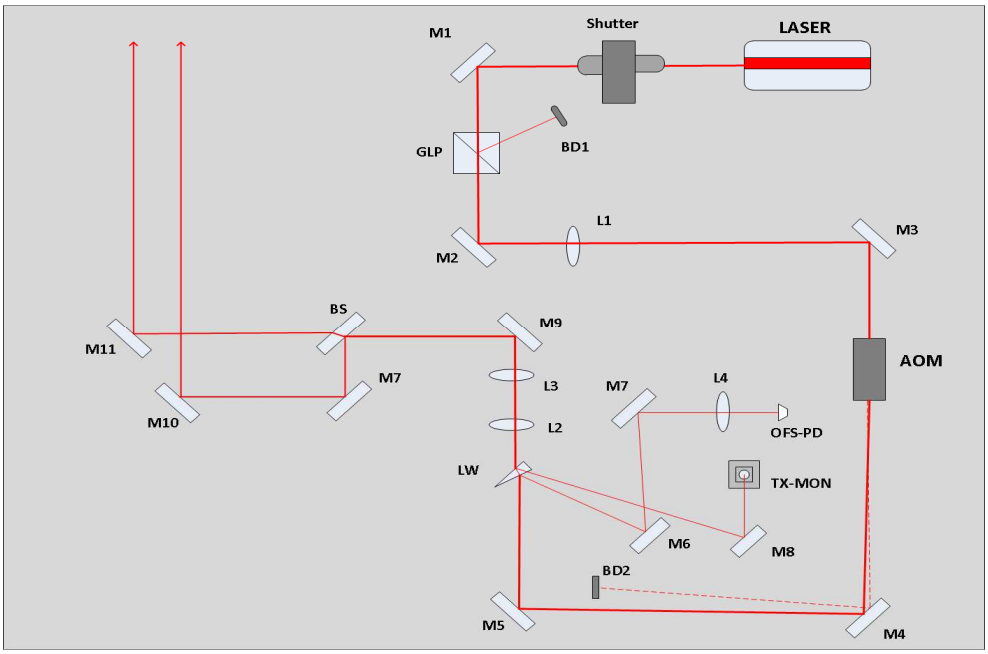

II. Harmonics amplitude for different modulation and for frequencies carrier of 50, 400, 1100 and 2000 Hz

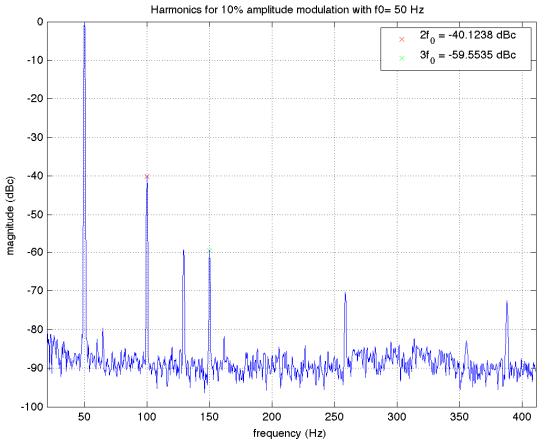

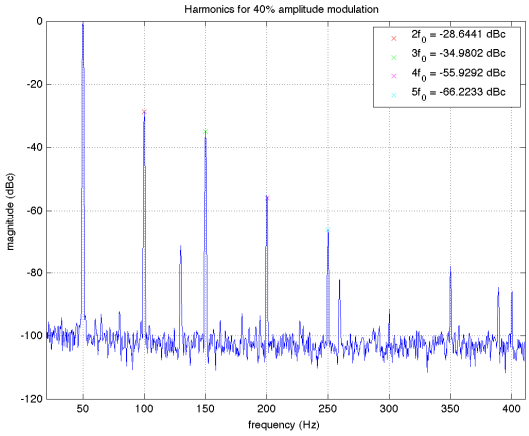

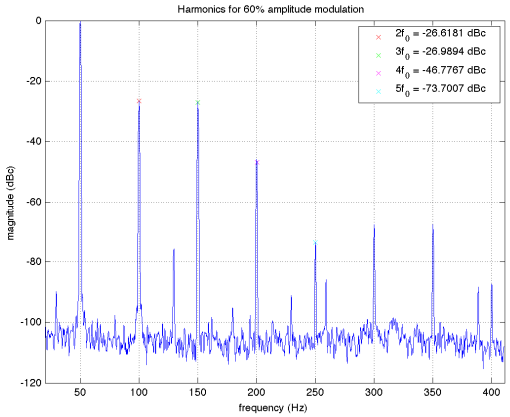
Harmonics for 60% amplitude modulation
2f0 = -26.6181 dBc
3f0 = -26.9894 dBc
4f0 = -46.7767 dBc
5f0 = -73.7007 dBc
magnitude (dBc)
frequency (Hz)

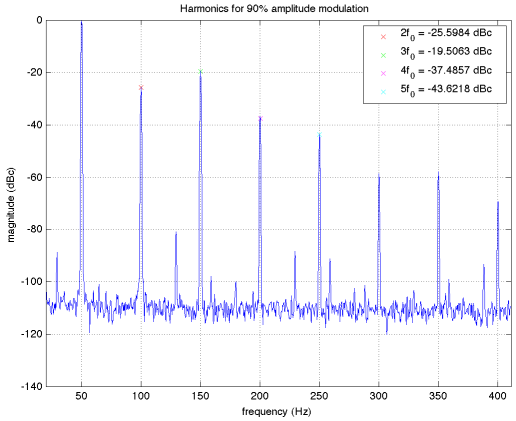
Harmonics for 90% amplitude modulation
2f0 = -25.5984 dBc
3f0 = -19.5063 dBc
4f0 = -37.4857 dBc
5f0 = -43.6218 dBc
magnitude (dBc)
frequency (Hz)

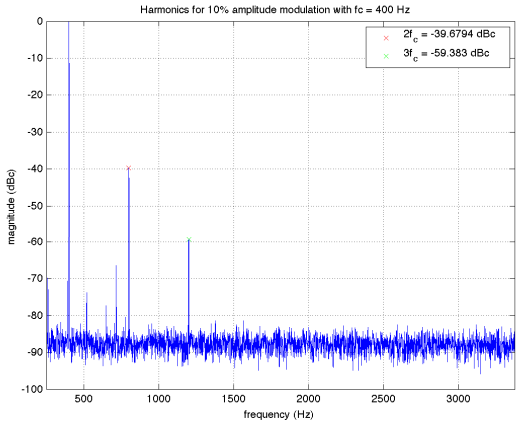
Harmonics for 10% amplitude modulation with fc = 400 Hz
2fc = -39.6794 dBc
3fc = -59.383 dBc
magnitude (dBc)
frequency (Hz)

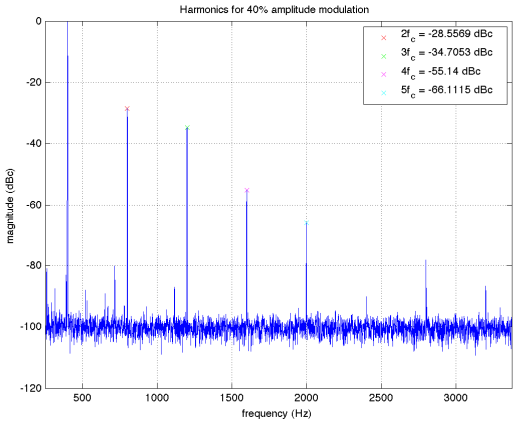
Harmonics for 40% amplitude modulation
2fc = -28.5569 dBc
3fc = -34.7053 dBc
4fc = -55.14 dBc
5fc = -66.1115 dBc
magnitude (dBc)
frequency (Hz)

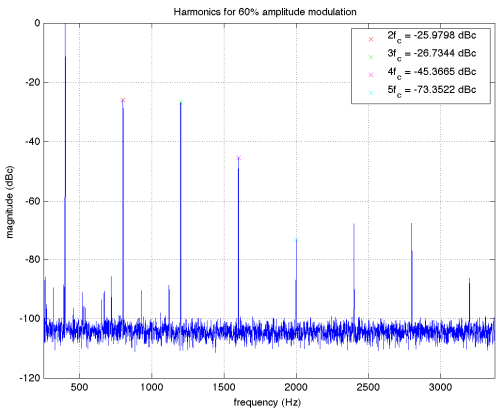
Harmonics for 60% amplitude modulation
2fc = -25.9798 dBc
3fc = -26.7344 dBc
4fc = -45.3665 dBc
5fc = -73.3522 dBc
magnitude (dBc)
frequency (Hz)

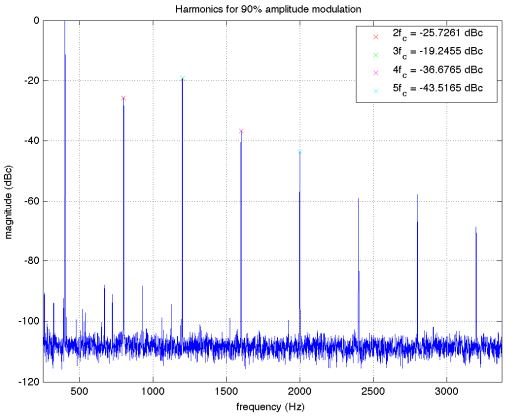
Harmonics for 90% amplitude modulation
2fc = -25.7261 dBc
3fc = -19.2455 dBc
4fc = -36.6765 dBc
5fc = -43.5165 dBc
magnitude (dBc)
frequency (Hz)

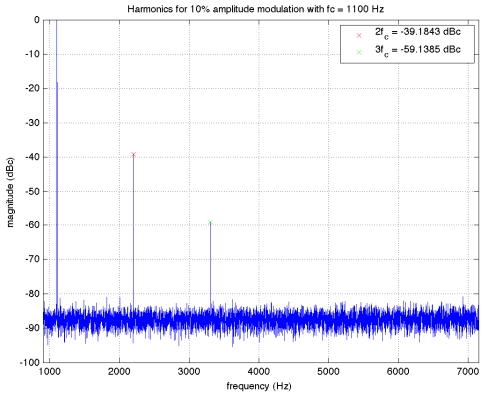
Harmonics for 10% amplitude modulation with fc = 1100 Hz
2f_c = -39.1843 dBc
3f_c = -59.1385 dBc
magnitude (dBc)
frequency (Hz)

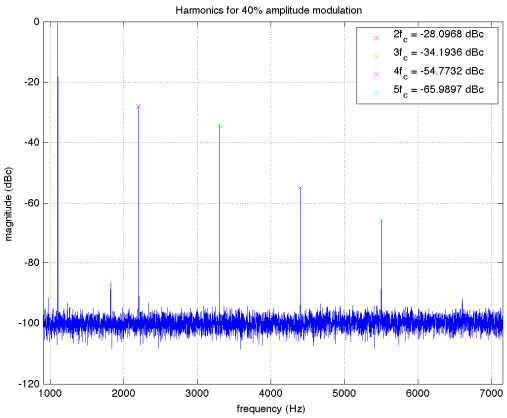
Harmonics for 40% amplitude modulation
2f_c = -28.0968 dBc
3f_c = -34.1936 dBc
4f_c = -54.7732 dBc
5f_c = -65.9897 dBc
magnitude (dBc)
frequency (Hz)

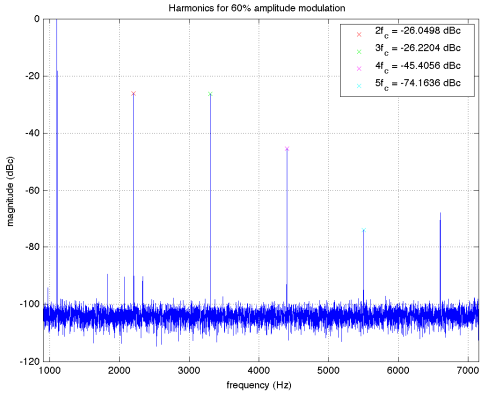
Harmonics for 60% amplitude modulation
2f_c = -26.0498 dBc
3f_c = -26.2204 dBc
4f_c = -45.4056 dBc
5f_c = -74.1636 dBc
magnitude (dBc)
frequency (Hz)

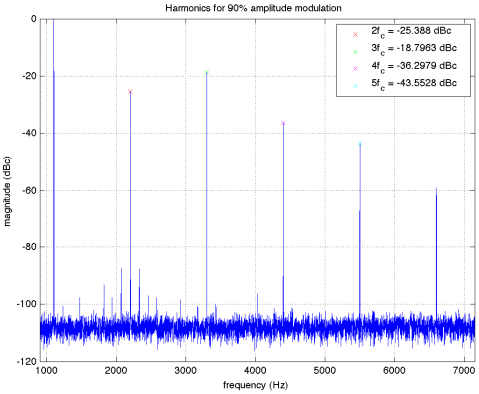
Harmonics for 90% amplitude modulation
2f_c = -25.388 dBc
3f_c = -18.7963 dBc
4f_c = -36.2979 dBc
5f_c = -43.5528 dBc
magnitude (dBc)
frequency (Hz)

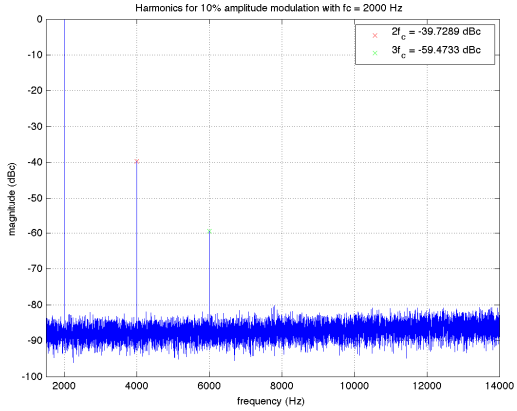
Harmonics for 10% amplitude modulation with fc = 2000 Hz
2f_c = -39.7289 dBc
3f_c = -59.4733 dBc
magnitude (dBc)
frequency (Hz)

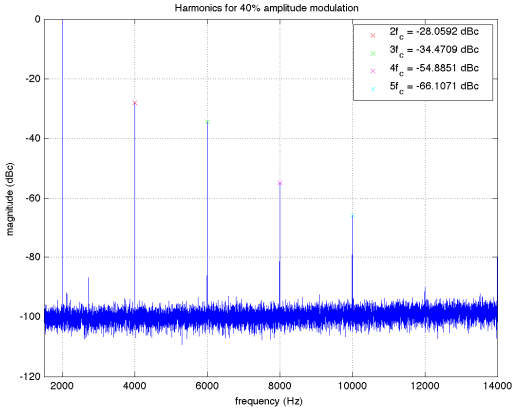
Harmonics for 40% amplitude modulation
2f_c = -28.0592 dBc
3f_c = -34.4709 dBc
4f_c = -54.8851 dBc
5f_c = -66.1071 dBc
magnitude (dBc)
frequency (Hz)

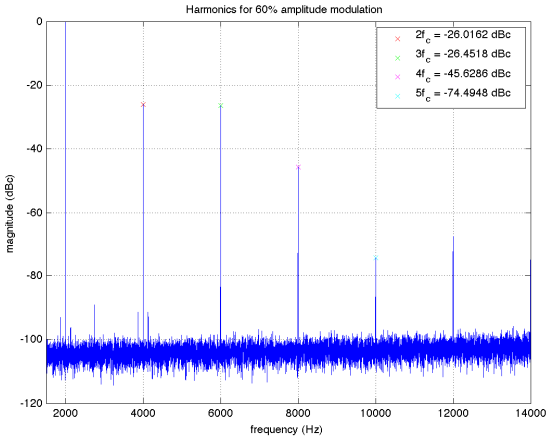

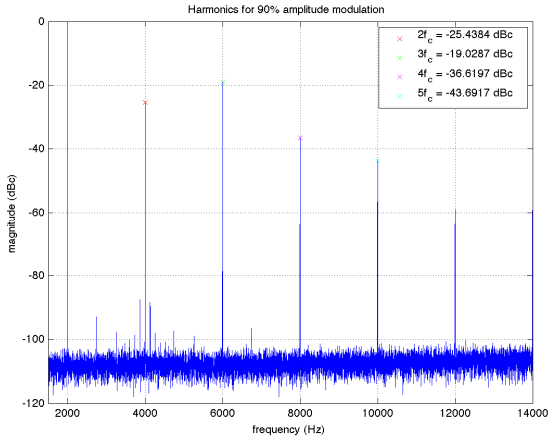

III. Amplitude of the carrier and harmonics for a square wave

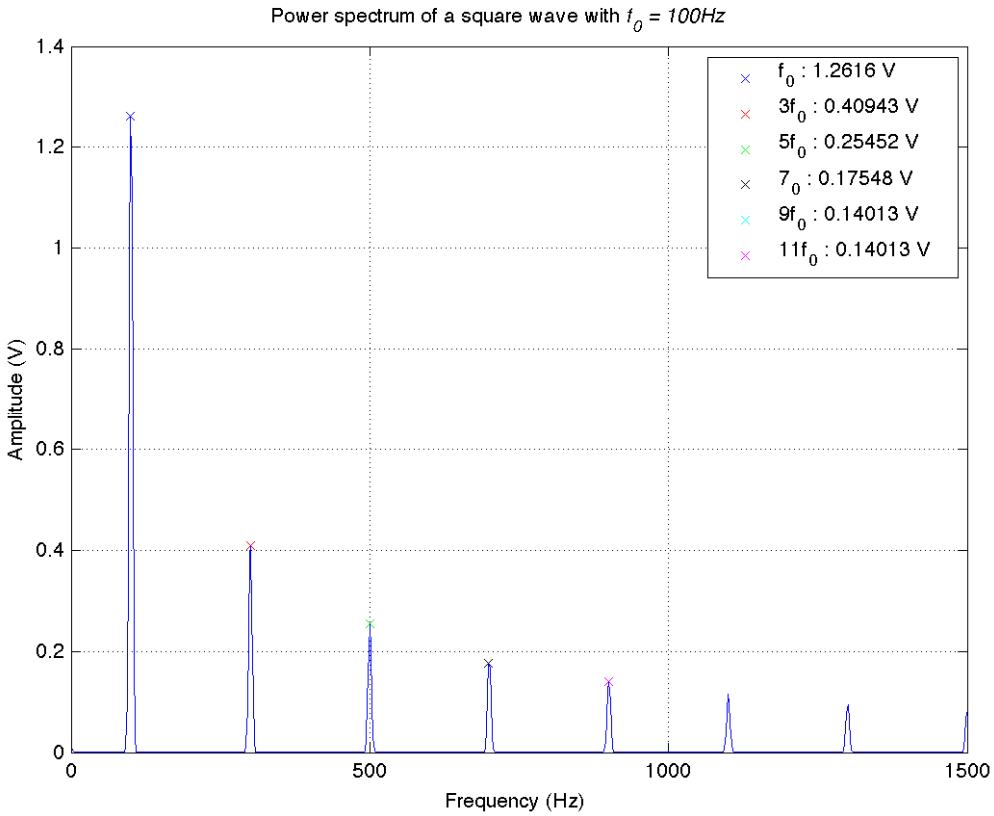

IV. Laplace transforms

Time domain	S domain
$\delta(t)$	1
$1(t)$	$1/s$
t	$1/s^2$
e^{-at}	$1/(s+a)$
$e^{-at}f(t)$	$F(s+a)$
$\sin(\omega t)$	$\omega/(s^2+\omega^2)$
$\cos(\omega t)$	$s/(s^2+\omega^2)$

V. A low pass filter

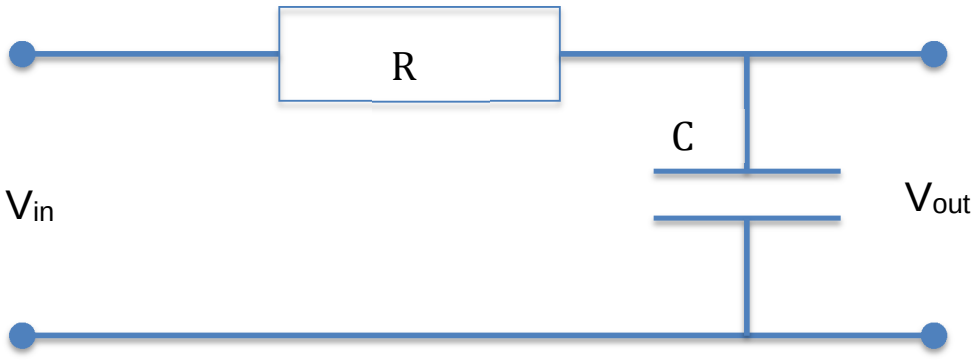

VI. Model of the Optical Follower Servo

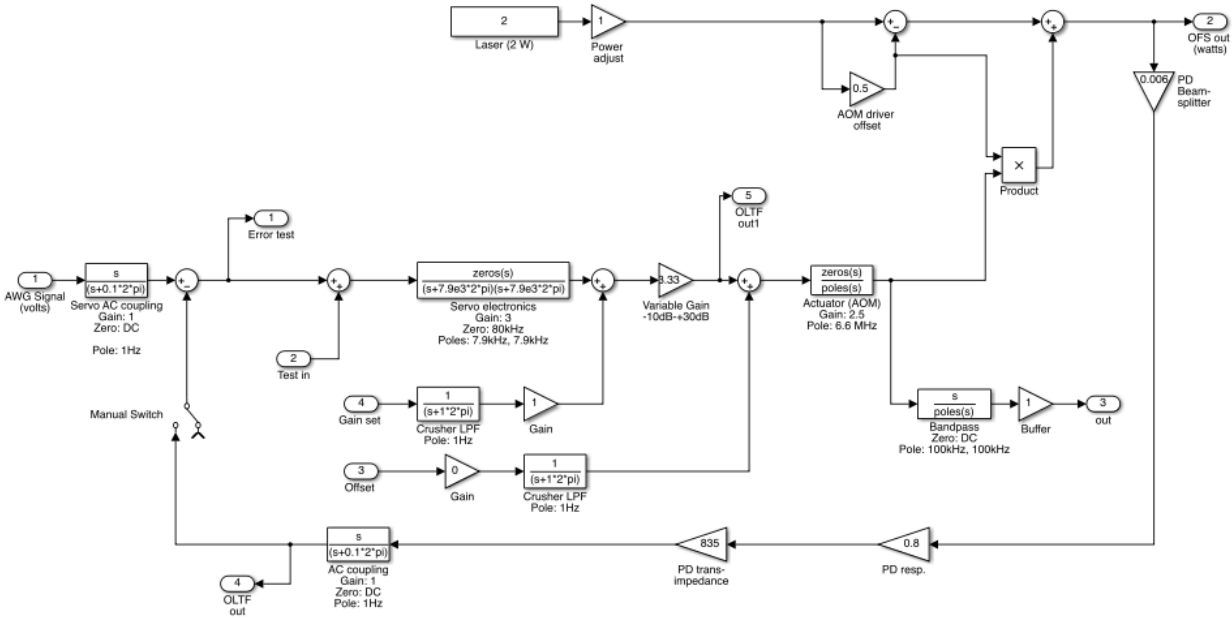

VII. Bode diagrams for 50 zero frequencies from 40 kHz (blue) to 120 kHz (red)

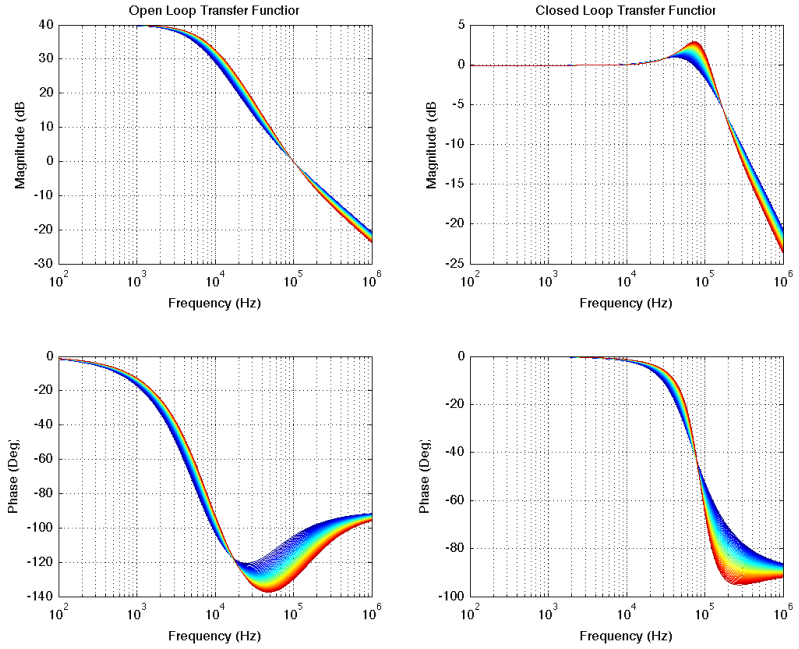

VIII. Open loop transfer function of the OFS model

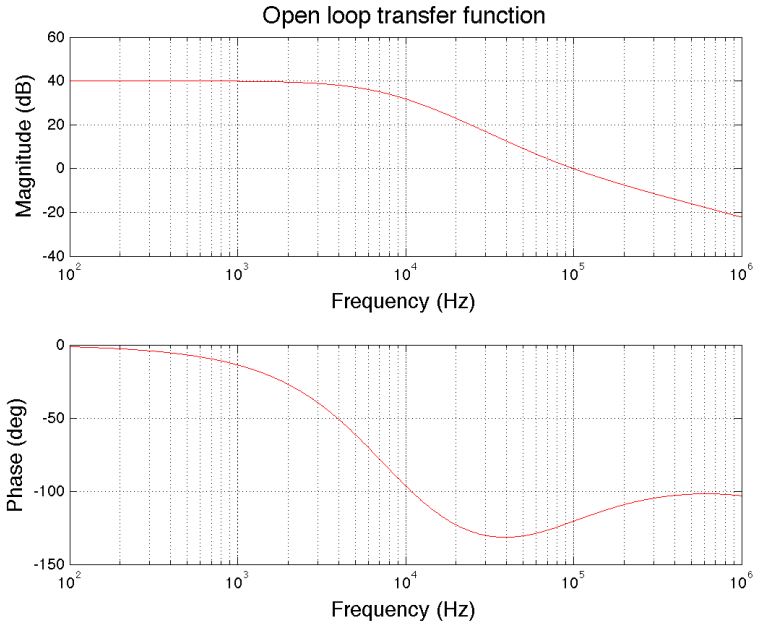

IX. Inversion of the polarity of the signal

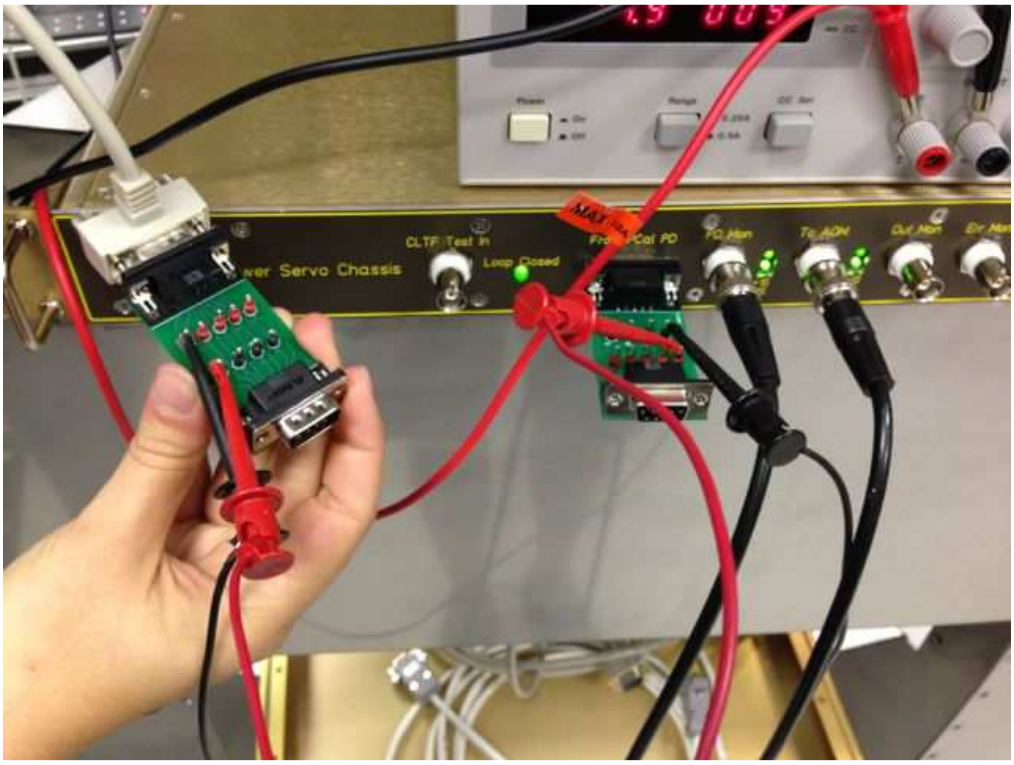

Bibliography

[1] Kip S. Thorne: *Three hundred years of gravitation*. Cambridge university press, 1987.

[2] Damir Buskulic: *Ondes gravitationnelles, aspects théoriques et expérimentaux*. http://lappweb.in2p3.fr/~buskulic/cours/Notes_cours_Buskulic_Jijel.pdf

[3] Joel M. Weisberg, Joseph H.Taylor: *Relativistic Binary Pulsar B1913+16: Thirty Years of Observations and Analysis*. ASP Conference Series, Vol. TBD, 2004.

[4] Loïc Villain: *Les ondes gravitationelles: la symphonie de l'espace-temps* .http://www.lmpt.univ-tours.fr/~loic/PDF/encas-gw.pdf

[5] R.W.P. Drever: *The detection of gravitational waves*. Cambridge university press, 1991.

[6] Lee Lindblom: *Optical Calibration Accuracy for Gravitational Waves Detector*. http://arxiv.org/pdf/0906.5153v2.pdf, *9 June 2013*

[7] E Goetz, P Kalmus, S Erickson, R L Savage Jr, G Gonzalez, K Kawabe, M Landry, S Marka, B O'Reilly, K Riles, D Sigg, P Willems: *Precise calibration of LIGO test mass actuators using photon radiation pressure.* Classical and Quantum Gravity, 2009.

[8] Jonathan Berliner, Richard Savage Jr: *Photon Calibrator Final Design.* https://dcc.ligo.org/DocDB/0032/T1100068/020/PhotonCalibratorFinalDesign.pdf, 24 February 2013.

[9] Gregorio Tellez, Richard Savage Jr: *Photon Calibrator: Optical Follower Servo Design Requirements.* https://dcc.ligo.org/DocDB/0101/T1300162/001/T1300162-V1.pdf, 26 February 2013

[10] Karl Johan Åström, Richard M.Murray: *Feedback Systems.* Princeton University Press, 2008.

[11] Yuri Panarin: *S-domain analysis: Poles, zeros, and Bode plot.* http://www.electronics.dit.ie/staff/ypanarin/Lecture%20Notes/K235-1/2%20s-Domain%20Analysis.pdf

[12] Joseph J.Distefano, III, Allen R. Stubberud, Ivan J.Williams: *Feedback on control system*. Schaum's outlines, 2nd edition, 1995.

[13] John Bechhoefer: *Kramers-Kronig, Bode, and the meaning of the zero.* July 4, 2011, http://arxiv.org/pdf/1107.0071v1.pdf

John Bechhoefer: *Feedback for physicists: a tutorial essay on control*. Review of modern physics, (77), July 2005.

Nicolas Yunes, Xavier Siemens: *Gravitational Wave Tests of General Relativity with Ground-Based Detectors and Pulsar Timing Arrays*

Boris J. Lurie, Paul J. Enright: *Classical Feedback Control with MATLAB and Simulink.* CRC Press, 2012.

Oleg A. Yakimenko: *Engineering Computations and Modeling in MATLAB/Simulink.* AIAA Education Series, 2011.